Simulations for experimental study of warm dense matter and inertial fusion energy applications on NDCX-II

J. J. Barnard[1], J. Armijo[2], F. M. Bieniosek[2], A. Friedman[1], M. Hay[2], E. Henestroza[2], B. G. Logan[2], R. M. More[2], P. A. Ni[2], L. J. Perkins[1], S-F. Ng[2,4], J.S. Wurtele[2], S.S. Yu[2,4], A. B. Zylstra[2]

[1]*Lawrence Livermore National Laboratory, Livermore, CA, USA*

[2]*Lawrence Berkeley National Laboratory, Berkeley, CA, USA*

[3]*Tech-X Corporation, Boulder, CO, USA*

[4]*Chinese University, Hong Kong, China*

E-mail: jjbarnard@llnl.gov

Abstract. The Neutralized Drift Compression Experiment II (NDCX II) is an induction accelerator planned for completion in 2012. The baseline design calls for a 3 MeV, 30 A Li^+ ion beam, delivered in a bunch with characteristic pulse duration of 1 ns, and transverse dimension of order 1 mm. The purpose of NDCX II is to carry out experimental studies of material in the warm dense matter regime, and ion beam/hydrodynamic coupling experiments relevant to heavy ion based inertial fusion energy. In preparation for this new machine, we have carried out hydrodynamic simulations of ion-beam-heated, metallic solid targets, connecting quantities related to observables, such as brightness temperature and expansion velocity at the critical frequency, with the simulated fluid density, temperature, and velocity. We examine how these quantities depend on two commonly used equations of state.

*This work was performed under the auspices of the U.S Department of Energy by Lawrence Livermore National Laboratory under Contract DE AC52 07NA27344, and by the University of California, Lawrence Berkeley National Laboratory under Contract DE AC03 76SF00098.

1. Introduction

Ion beams have a number of advantages for heating materials to the Warm Dense Matter (WDM) state [1 - 4]. Included among these are capabilities for spatially uniform and volumetric energy deposition over relatively large and diagnosable material volumes. The Neutralized Drift Compression Experiment (NDCX II) is now being constructed at Lawrence Berkeley National Laboratory to study Warm Dense Matter questions and to investigate target-beam coupling relevant to heavy-ion driven inertial fusion energy. NDCX II is the successor to the experiment NDCX I that demonstrated the technique of injecting plasma into the final beam path to greatly reduce the effects of space charge and therefore achieve short pulses needed for WDM and IFE studies [5]. The physics design of the NDCX II accelerator is described elsewhere [6]. In section 2, we review the target configurations considered for NDCX II. In section 3, we give an example of a particular simulation of a solid Aluminum foil target. In section 4, we examine the expected temperature and velocity at the critical surface that are related to measurements of an instantaneously heated ideal gas. In sections 5 and 6 we examine predictions of the same measurements derived from simulations of a more realistic equation of state, heated over a finite pulse duration with realistic ion deposition by a beam. Finally, in section 7 we summarize our results.

2. Target configurations for NDCX II

A number of target configurations have been considered for NDCX II. These include spherical [7] and cylindrical bubbles [8] (to create enhanced regions of higher pressure and temperature) and planar solid and planar foam [9] targets. Pulse formats include single pulses of fixed ion energy (but with an energy spread at the target) for WDM studies, and double pulses with varied energy (or single pulses with ion energy that changes over the pulse) to investigate ion-coupling efficiency[10]. Recent heavy ion driven "direct drive" target simulations for inertial fusion energy have shown promisingly high fusion gain [11], by increasing the range over the course of the pulse. This increasing range can be accomplished by increasing the ion energy over the course of the pulse. Experiments that demonstrate increased coupling efficiency by increasing the range over the course of the pulse have been simulated[10]. In this paper, however, we focus on the WDM mission for NDCX II.

3. Simulation of beam-heated solid aluminum target

As described in section 2, NDCX II is being designed to heat both solid and porous planar metallic foils, among other options. For the simulations described in this paper we used the radiation hydrodynamics code HYDRA [12]. We assumed the target material was a 3.5 μm thick solid Aluminum, and that the equation of state was either QEOS [13] or LEOS (see fig. 1), both of which are accessible by the HYDRA code. The ion intensity varied with time as a parabola of full width duration 1 ns. The ion beam used was a 2.8 MeV Li^+ beam and the simulation used HYDRA's Bethe-Bloch ion deposition algorithm. The intensity was adjusted to yield approximately 20 kJ/g integrated over the pulse. The HYDRA simulations were 2D with an assumed 0.5 mm beam radius; the results here simply describe the 1D evolution of the target along the longitudinal axis (parallel to the beam direction). Figure 2 describes the evolution of the density, temperature, velocity, and charge state Z* of the target during the 1 ns of heating of the pulse.

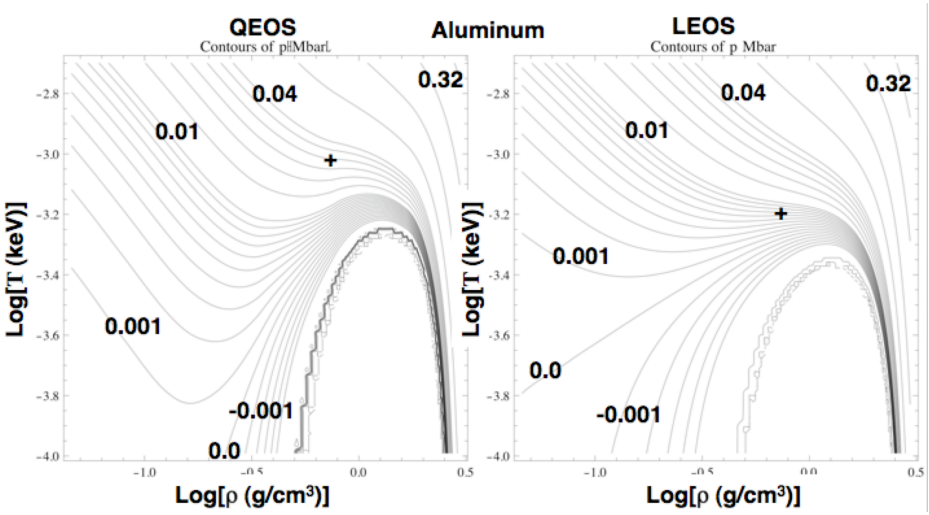

Figure 1. Isobars of pressure (in MBar) as a function of temperature and density for two different equations of state used by the HYDRA code (QEOS and LEOS). Crosses indicate location of critical point.

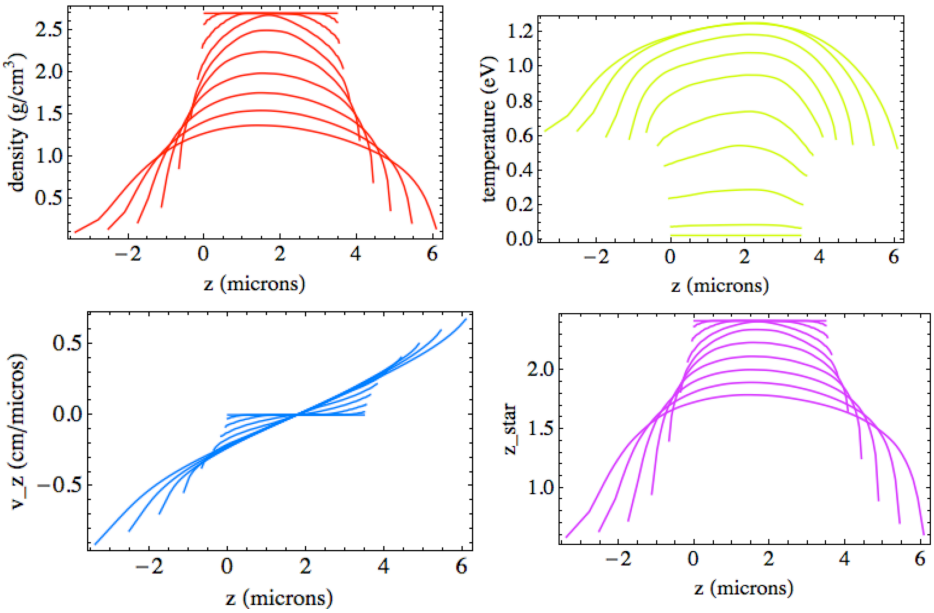

Figure 2. Longitudinal variation of target at radial center (r=0) for ten different times equally spaced between 0 and 1 ns. Ion beam heating ends at 1 ns. Target initially lies between 0 and 3.5 microns. Upper left: Density vs. longitudinal distance z; Upper right: Temperature kT vs. z. Lower left: Longitudinal velocity v_z vs. z; Lower right: Effective charge state of target Z^* vs. z.

4. Instantaneously heated, idealized slab

As a way of qualitatively understanding foil expansion we may look at the analytic solution to the idealized problem of a foil that is instantaneously heated, has an ideal gas equation of state and expands isentropically [14, 15]. In this case, a rarefaction wave propagates inward at the initial sound speed c_s of the foil (calculated using the

initial temperature after instantaneously heating but before any expansion). The front of the relaxation wave propagates outward at $2c_s/(\gamma\text{-}1)$, equal to $3c_s$ for a perfect monatomic gas, for which the ratio of specific heats $\gamma=5/3$. It is useful to calculate the critical frequency as a function of the longitudinal position. For a particular emission frequency ν, light propagation becomes evanescent when the frequency falls below the critical frequency ν_{crit} in the medium (equal to the angular plasma frequency ω_p in the medium divided by 2π). This relation can be written,

$$h\nu_{crit} = h\omega_p/2\pi = 28 \text{ eV } \sqrt{\rho(\text{g/cm}^3)Z^*/A_{\text{target}}} \qquad (1)$$

Here Z^* is the effective charge state of the medium, ρ is the mass density and A_{target} is the atomic mass number of the target. If we further assume in this example that Z^* is fixed, it is apparent that lines of constant critical frequency are coincident with lines of constant density. Further, the assumption of instantaneous heating implies that all fluid elements have the same entropy equal to their initial value. For such a fluid, the pressure P can be written as a function only of the density ρ, $P = K\rho^\gamma$ and it follows that $T \sim \rho^{\gamma-1}$, and so lines of constant temperature are coincident with lines of constant density. If we model the emission from such a slab, by assuming emission at the blackbody intensity from the location of the critical frequency, we can get a qualitative picture of the emission evolution as a function of time. If at a given frequency, the critical frequency for all parts of the slab lies below the observation frequency, we assume that the observed intensity will be that at the maximum (central) temperature in the slab. (In fact, an integration that includes contributions from all portions of the slab is appropriate and in order. Here we simply assume the steep temperature dependence on emission will dominate the emergent spectra.) Figure 3 shows the trajectory in the z, t plane of the constant density surface. It is clear that for sufficiently low observation frequencies, the point of emission will first propagate outward and then plunge toward the axis. During this time, the brightness temperature will be constant (since the temperature will be constant along the density contour), and a "plateau" in the emission will be observed.) The length of the plateau will be dependent on the frequency of the emission. From the approximate analytic formula in ref. [12] we find that the central density ρ_{center} evolves with time t as:

$$\frac{\rho_{center}}{\rho_0} = \frac{3}{2}\left(1 - \frac{1}{\tau^{1/2}} + \frac{1}{3\tau} - \frac{1}{3\tau^{3/2}}\right)/(3\tau - 4\tau^{1/2} + 1) \qquad (\tau > 1) \qquad (2)$$

Here we have again assumed a $\gamma=5/3$ perfect gas, $\tau\,(= c_s\,t/L)$ is the time measured in hydrodynamic timescales L/c_s, and the formula is valid for $\tau > 1$. (For $\tau < 1$, $\rho_{\text{center}} = \rho_0$). For $\tau >> 1$, eq.[2] reduces to $\rho_{center}/\rho_0 \approx 1/(2\tau)$. This implies that the duration Δt of the constant density contour varies according to density as $\Delta t \approx L\rho_0/(2\rho c_s)$, and since $\nu_{crit} \sim (\rho Z^*)^{1/2}$ then $\Delta t \sim L\,\nu_{crit0}{}^2 Z^{*2}/(2L\,\nu_{crit}{}^2 Z_0^{*2} c_s)$, and the condition $\tau >> 1$, requires that $\nu_{crit0}Z_0^*/(\nu_{crit}Z^*) >> 1$. Here subscript 0 indicates a quantity right after the instantaneous heating (t=0). If Z^* is constant, then the low frequency observers of emission from the critical surface will see constant emission for a timescale that is longer than the hydrodynamic timescale by a factor $(\nu_{crit0}/\nu_{crit})^2$. The temperature of material at the critical frequency is given by $T/T_0 = (\rho/\rho_0)^{2/3} = (\nu_{crit}Z_0^*/[\nu_{crit0}Z^*])^{4/3}$.

As an example, if the initial central critical frequency (times Planck's constant) is 14 eV, and the initial central temperature is 2 eV, an observer of an infrared photon energy of 0.8 eV would observe that the critical surface would have (assuming $Z_0^*/$

$Z^*=1$) a temperature of 0.04 eV, and it would remain at a constant intensity for 306 hydrodynamic times L/c_s. In more realistic situations, as the density is lowered, Z* is lowered, so that the temperature is not as low, and the time duration is not as long.

As can be seen from figure 3, initially the velocity contours overlie the density contours so that for a time the velocity of the critical surface is constant. However, after the time at which the density contour plunges towards the axis $z/L=1$ (at the boundary between the so-called simple and non-simple wave solution), the density contours are crossing the velocity contours, so that during this "plunge" the velocity of the critical surface tends towards zero, the value it reaches when it reaches the center of the target ($z/L=1$). During the initial evolution, under the same assumptions as above, the velocity of the critical surface satisfies: $v= 3\, c_s\, ((\nu_{crit} Z_0^* / [\, \nu_{crit0} Z^*])^{2/3} - 1)$. Using the same parameters as the example above the velocity of the 0.8 eV (IR) surface would have maximum magnitude 2.55 c_s and then tend to zero at 306 L/c_s (at the end of the plateau in T).

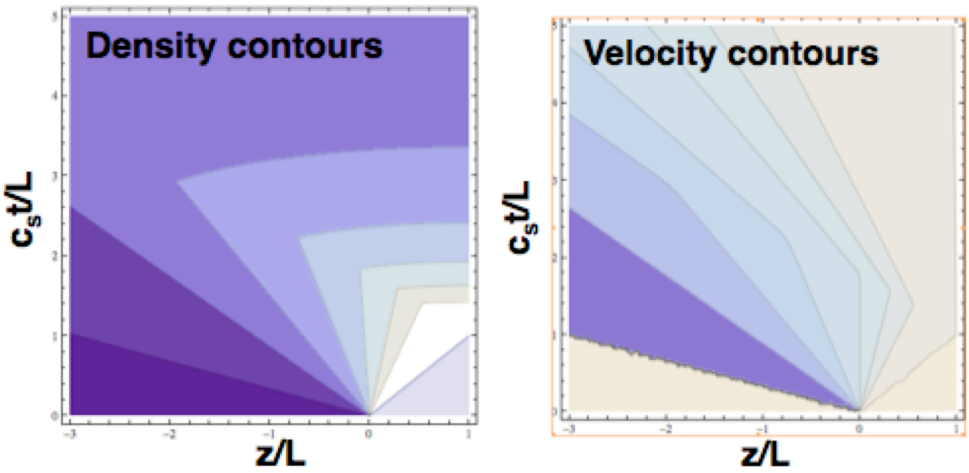

Figure 3. Density (left) and velocity (right) contours as a function of longitudinal position and time. Here the instantaneously heated foil is located between $z=0$ and $z=2L$, with only the left half-plane shown. The right half plane is a mirror reflection. The quantity c_s is the initial sound speed (after the instantaneous heating occurs at $t=0$).

5. Predicted brightness temperature evolution for beam heated Aluminum target

For the target that is heated in a finite pulse duration, with finite non-uniformity, with a non-ideal gas equation of state, and an evolving Z*, the evolution will differ from that described in section 4. As a way of testing the ability of pyrometer measurements [15] to discriminate equations of state in an actual experiment, we estimated the temperature as a function of time as measured by a pyrometer at three widely separated wavelengths, using the ion pulse parameters and two EOS's described in section 3. For the brightness temperature, we again assume the following model for the brightness temperature T_b:

$$T_b = \begin{cases} T_{\max} & \text{if} \quad \nu > \nu_{crit\,\max} \\ T(\nu_{crit}) & \text{if} \quad \nu_{crit\,\max} > \nu > \nu_{crit\,\min} \\ 0 & \text{if} \quad \nu_{crit\,\min} > \nu \end{cases} \tag{3}$$

Here T_{max} is the maximum material temperature within the foil (generally found at the foil center), $\nu_{critmax}$ is the maximum critical frequency in the foil (also usually at the center) and $\nu_{critmin}$ is the minimum critical frequency in the simulation (usually at the outermost zone, numerically limited by the finite density of the lagrangian fluid element). The results for the NDCX II simulations are found in figs. 4 and 5.

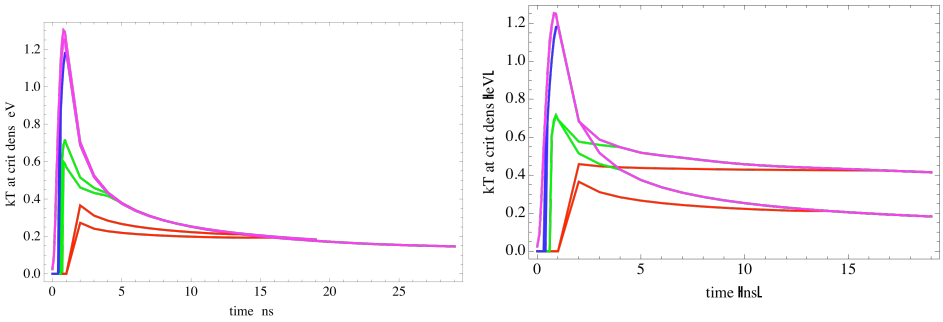

Figure 4. Left: Evolution of brightness temperature (defined in eq. 3) for three observation photon energies (red: 1500 nm; green 450 nm, and blue: 150 nm) and two equations of state (upper: LEOS; lower: QEOS). Both EOS are without Maxwell construction. The magenta curve is the evolution of T_{max}. Right: Same as left figure, except that the upper curves are LEOS without Maxwell construction, and the lower curves are with the Maxwell construction.

6. Predicted velocity evolution for beam heated Aluminum target

We may similarly calculate the velocity that would be inferred by a reflected laser pulse if the reflection occurs predominantly at the critical frequency. These results are shown in figure 4.

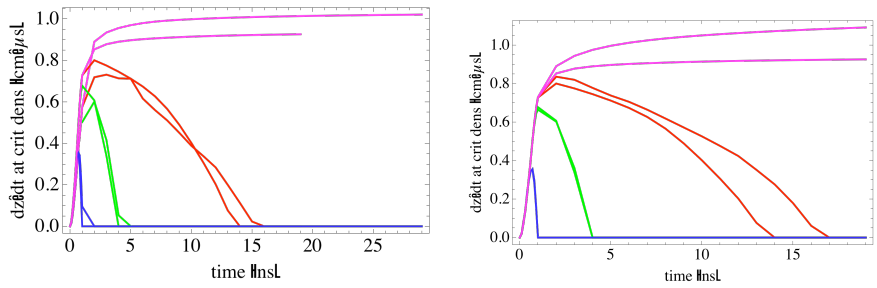

Figure 4. Left: Evolution of velocity at the critical density for three observation photon energies (red: 1500 nm; green 450 nm, and blue: 150 nm) and two equations of state (upper: LEOS; lower: QEOS). Both EOS are without Maxwell construction. The magenta curve is the evolution of v_{max}, the velocity of the outermost zone. Right: Same as left figure, except that the upper curves are LEOS without Maxwell construction, and the lower curves are with the Maxwell construction.

7. Discussion and conclusion

It is evident from figures 3 and 4 that widely spaced wavelength pyrometry measurements of expanding foils will differ at the 15 to 25% level, between the two equations of state (QEOS and LEOS) that have differences as shown in Fig. 1. The qualitative results of section 4 are confirmed. Namely, the brightness temperature is lower at lower frequencies and the pulse duration is longer. It is also worth noting that the choice of whether to use the Maxwell construction in hydrodynamic simulations also makes significant and measurable differences to predicted pyrometry measurements, particularly in the IR for these parameters. The choice of which construction to use is non-trivial. Maxwell construction implies equilibrium has occurred over the length scale of the simulation zone, even in the dynamically changing situation of a rapidly expanding foil. Simulation without the Maxwell construction implies that droplets and bubbles are well resolved, which is unlikely to be true at all scales [16].

For the velocity measurements, the differences between EOS (and between simulations with and without Maxwell construction) are most clearly seen in the longer wavelength results; the differences are on the 10% level for the two candidate EOS's.

We should point out that these calculations have neglected any absorption through the medium and any differences between the propagation of the two polarization states, and so are really only a first look at the ability of NDCX II to clarify EOS questions. We have also used a solid target as the most rigorous test, as the hydrodynamic time scale for this case is the shortest relative to the pulse duration of NDCX II. Including these additional physics and a wide range of materials is currently under study by the authors. Finally we should note that these calculations can also be applied to (and were partially motivated by) laser heated targets if there is initial temperature equilibration followed by hydrodynamic expansion [17].

8. References

1. B.G. Logan, et al., "Heavy ion fusion science research for high energy density physics and fusion applications," IFSA 2007, Journal of Physics, Conference Series 112 (2008) 032029.
2. N.A. Tahir, P. Spiller, S. Udrea, O.D. Cortazar, C. Deutsch, V.E. Fortov, V. Gryaznov, D.H.H. Hoffmann, I.V. Lomonosov, P. Ni, A.R. Piriz, A. Shutov, M. Temporal, D. Varentsov," Studies of equation of state properties of high-energy densitymatter using intense heavy ion beams at the future FAIR facility: The HEDgeHOB collaboration," Nuclear Instruments and Methods in Physics Research B 245 (2006) 85–93.
3. J.J. Barnard, et al., Accelerator and ion beam tradeoffs for studies of warm dense matter, Proc. 2005 Particle Accelerator Conference, p. 2568 (2005).
4. F.M. Bieniosek, E. Henestroza, M. Leitner, B.G. Logan, R.M. More, P.K. Roy, P. Ni, P.A. Seidl, W.L. Waldron, J.J. Barnard, High energy density physics experiments with intense heavy ion beams, Nucl. Instrum. Meth. A 606 (2009) 146-151.
5. P.A. Seidl, A. Anders, F.M. Bieniosek, J.J. Barnard, J. Calanog, A.X. Chen, R.H. Cohen, J.E. Coleman M. Dorf, E.P. Gilson, D. P. Grote, J.Y. Jung, M. Leitner, S.M. Lidia, B.G. Logan, P. Ni, P.K. Roy, K. van den Bogert, W.L. Waldron, D.R. Welch, Progress in beam focusing and compression for warm-dense-matter experiments, Nucl. Instrum. Meth. A 606 (2009) 75-82.

6. A. Friedman *et al*., Nucl. Instr. and Meth. A **606**, 6 (2009).
7. S. F. Ng, J. J. Barnard, P. T. Leung, B.G. Logan, and S. S. Yu, in preparation (2009).
8. J. J. Barnard, J. Armijo, D. S. Bailey, A. Friedman, F. M. Bieniosek, E. Henestroza, I. Kaganovich, P. T. Leung, B. G. Logan, M.M. Marinak, R. M. More, S. F. Ng, G. E. Penn, L. J. Perkins, S. Veitzer, J. S. Wurtele, S. S. Yu, A. B. Zylstra, "Ion beam heated target simulations for warm dense matter physics and inertial fusion energy," Nuclear Instruments and Methods in Physics Research A, **606**, 134-138, (2009)
9. A. B. Zylstra, J.J. Barnard, and R. M. More, in preparation (2009).
10. S. F. Ng, S. Veitzer, J. J. Barnard, P. T. Leung, S. S. Yu, in preparation (2009).
11. B. G. Logan, L. J. Perkins, and J. J. Barnard, Phys. Plasmas **15**, 072701 (2008).
12. J. J. Barnard, J. Armijo, R. M. More, A. Friedman, I. Kaganovich, B. G. Logan, M. M. Marinak, G. E. Penn, A. B. Sefkow, P. Santhanam, P. Stoltz, S. Veitzer, J. S. Wurtele, "Theory and Simulation of Warm Dense Matter Targets," Nuclear Instruments and Methods in Physics Research A, 577 (2007) 275-283.
13. R. More, K.H. Warren, D.A. Young, G. B. Zimmerman, "A new quotidian equation of state for hot dense matter", Phys. Fluids, **31**, 3062 (1988).
14. L.D. Landau and E.M. Lifshitz, "Fluid Mechanics," Pergamon Press (chapter 10) (1959).
15. P.A. Ni, M.I. Kulish, V. Mintsev, D.N. Nikolaev, V.Ya. Ternovoi, D.H.H. Hoffmann, S. Udrea, A. Hug, N.A. Tahir, D. Varentsov, "Fast six-channel pyrometer for warm-dense-matter experiments with intense heavy-ion beams", Laser and Particle Beams, December 2008.
16. J. Armijo and J.J. Barnard, in preparation (2009).
17. P. A. Ni, F. M. Bieniosek, M. Leitner, C. Weber, W. L. Waldron, "Testing of optical diagnostics for ion-beam driven WDM experiments on NDCX-I," Nuclear Instruments and Methods in Physics Research A, **606**, (2009), 169-171.